Postprint of: Lech R., Marynowski W., Kusiek A., Mazur J., An Analysis of Probe-Fed Rectangular Patch Antennas With Multilayer and Multipatch Configurations on Cylindrical Surfaces, IEEE Transactions on Antennas and Propagation, Vol. 62, Iss. 6 (2014), pp. 2935-2945, DOI: 10.1109/TAP.2014.2313137

An Analysis of Probe-fed Rectangular Patch Antennas with Multi-layer and Multi-patch Configurations on Cylindrical Surfaces

Rafal Lech, Wojciech Marynowski, Adam Kusiek, and Jerzy Mazur

***Abstract*—A multi-patch configuration of probe-fed rectangular microstrip antennas mounted on a cylindrical body, with electrically small radius, with an arbitrary number of substrate and superstrate layers is investigated in this paper. A full-wave analysis and a moment-method calculation are employed. A unified procedure for creating proper matrices for the investigated geometry of the structure is outlined here. Numerical results for the input impedances and radiation patterns are calculated and verified by comparing them with results from the literature and our own measurements of manufactured prototypes.**

***Index Terms*—Microstrip antenna arrays, cylindrical antenna, probe feed, input impedance, antenna radiation patterns.**

I. Introduction

CONFORMAL antennas are interesting due to the possibility of their merging into curved surfaces. They find many practical applications in airplanes, spacecraft, speedboats and other high-speed vehicles where aerodynamic or hydrodynamic considerations necessitate their use. They can also be used on the facade of historic buildings, towers or columns as a part of a mobile communications system of a wireless base station, which is dictated by aesthetic considerations and the need to integrate the antenna with local architecture. Another advantage of utilizing conformal antennas arises from electromagnetic consideration and the need to obtain the specific performance of radiation characteristics. Antennas with curved surfaces provide a higher visible range relative to planar antennas. An example of such a structure is a circular antenna array or an array of radiators located on the surface of a cylinder, which provide omni-directional radiation patterns in the azimuth plane or else provide, in this plane, the possibility of beam control [1].

There are many different methods for analyzing antennas with cylindrical geometry. In the conformal antenna analysis, the methods are commonly divided according to the point of view of antenna dimensions (i.e., electrically small and electrically large antennas). The choice of the right method depends on the complexity of the structure geometry. Electrically small antennas are often analyzed using orthogonalization and mode-matching methods [2]- [6], the method of moments combined with integral equations [7]- [20], the finite element method, often combined with other approaches [21], [22], and the finite difference time domain method [23]- [25]. Although, the aforementioned solutions work well for electrically small cylinders, a closed-form solution for the analysis of a cylindrical microstrip antenna based on the spectral-domain method of moments, which works for an arbitrary radius of a cylinder, was proposed in [12]. The large antennas are often analyzed with the use of a high frequency approach, which uses various asymptotic techniques to find approximate solutions. In these approaches the antennas must be smooth and electrically large. The most popular and effective method is the uniform theory of diffraction, which uses the concept of light and describes the behavior of the wave propagating on curved surfaces. To take into account small details in the antenna structure geometry, this method is often combined with the method of moments [26]- [29].

In this paper, a configuration of probe-fed cylindrical-rectangular microstrip patch antennas mounted on electrically small-radius cylinders with an arbitrary number of substrate and superstrate layers is investigated. Single antenna configurations have been investigated in the past for a particular number of substrates and superstrates. The complex resonant frequency problem was studied, e.g., in [14], for a single substrate antenna, in [17] for a structure with an air gap under the substrate, and in [16] for a structure with a superstrate layer. The input impedance and radiation pattern of a probe-fed cylindricalrectangular microstrip patch were analyzed in [15] for a single substrate structure and in [19] for a superstrate-loaded antenna. The aforementioned analyses are valid only for the considered structures. In [13], an antenna with an arbitrary number of substrate and superstrate layers was investigated where real resonance frequencies and radiation patterns were calculated.

Here, we utilize a full-wave analysis and a moment-method calculation and propose a unified procedure of creating proper matrices for a multi-layer configuration of the probe-fed cylindrical-rectangular microstrip patch antennas. The procedure for the investigated configuration is outlined in section II and studied in detail in the appendix. In contrast to the aforementioned works of others, which are valid only for the specific antenna structures, the presented procedure allows to investigate the structures with any number of substrate and superstrate layers and any number of radiators localized within these layers. The procedure allows constructing proper matrices only by defining the structure geometry (number of

R. Lech W. Marynowski, A. Kusiek and J. Mazur are with the Department of Microwave and Antenna Engineering, Faculty of Electronics, Telecommunications and Informatics, Gdansk University of Technology, Gdansk, 80-233 Poland e-mail: rafal.lech@eti.pg.gda.pl, wojmar@eti.pg.gda.pl, adakus@eti.pg.gda.pl, jem@pg.gda.pl.

This work was supported from sources of National Science Center under grant decision no. DEC-2011/01/D/ST7/06639.

Manuscript received MMMM DD, 2013; revised MMMM DD, 2013.

substrate and superstrate layers, number and localization of radiators). Calculating the proper matrices for the antenna structure with, e.g., additional superstrate cover or an air gap in the substrate layer can be performed, with proposed procedure, automatically without the need to perform additional mathematical transformations. Therefore, the presented procedure can be utilized, e.g., in simulators for fast redefining the structure. The input impedances and radiation patterns for the chosen examples are calculated and the results are verified by comparing them with those presented in the literature and our own measurements of manufactured prototypes.

II. Formulation of the problem

The investigated structure is composed of Ξ ($\xi = 1, \ldots, \Xi$) patch antennas located on Ψ ($\psi = 1, \ldots, \Psi$) cylindrical surfaces with a cylinder axis along the $\vec{i}_z$ direction, as schematically illustrated in Fig. 1. Each patch is of length L_ξ (along the z axis) and width W_ξ (along the ϕ axis), and is located arbitrarily on the cylindrical surface, i.e., between ϕ_ξ and ϕ'_ξ along the ϕ axis and between z_ξ and z'_ξ along the z axis on the surface with a radius $r_{\kappa\psi}$. There can be several patch antennas on each surface and the antennas can be located above several dielectric substrates and covered by several dielectric superstrates with a total number of K layers with permittivities $\varepsilon_{r\kappa}$ ($\kappa = 1, \ldots, K$).

The patch antennas are excited by probe feeds located at $(\phi_{f\xi}, z_{f\xi})$, pointing along the $\vec{i}_\rho$ direction and extending from $\rho = r_1$ to $\rho = r_{\kappa\xi}$. With a very small radius of the probe (in comparison to the wavelength), the probe feed can be approximately treated as a line source with a current density:

$$J(\rho) = \frac{I_{f\xi}\delta(\phi - \phi_{f\xi})\delta(z - z_{f\xi})}{\rho}\vec{i}_\rho, \qquad r_1 \le \rho \le r_{\kappa\xi} \quad (1)$$

where $I_{f\xi}$ is the amplitude of the input current. It is assumed that the patches are made of an ideal conductor and, therefore, on the patch surfaces the tangential components of the electric field are zero. Utilizing this condition the unknown surface currents on the patches can be found. On the patches, the total electric field can be written as a superposition of the electric field due to the current distribution on the patches $\vec{E}^{patch}$ and due to the probe currents $\vec{E}^{feed}$ with the patch being absent [15]. The z components of the electric and magnetic fields, due to the current distribution on the patch in each region, have the following form (suppressing $e^{-i\omega t}$ time dependence):

$$F_z^{patch}(\rho,\phi,z) = \frac{1}{2\pi}\sum_{\nu=-\infty}^{\infty} e^{i\nu\phi}\int_{-\infty}^{\infty} dk_z e^{ik_z z} \times$$

$$\begin{cases} \left(H^\rho_{\nu 1} - \beta_1^\zeta J^\rho_{\nu 1}\right) A^\zeta_{\nu 1} & r_1 \le \rho \le r_2 \\ H^\rho_{\nu\kappa} A^\zeta_{\nu\kappa} + J^\rho_{\nu\kappa} A^{'\zeta}_{\nu\kappa} & r_\kappa \le \rho \le r_{\kappa+1} \\ \qquad \kappa = 2, \ldots, K-1, & \\ H^\rho_{\nu K} A^\zeta_{\nu K} & r_K \le \rho \end{cases} \quad (2)$$

where $F^{patch} = \{E^{patch}, H^{patch}\}$, $\zeta = \{e, h\}$ $A^\zeta_{\nu\kappa}$ and $A^{'\zeta}_{\nu\kappa}$ are unknown coefficients of the harmonic order ν. $\beta_1^e = H^{r_1}_{\nu 1}/J^{r_1}_{\nu 1}$ and $\beta_1^h = H^{'r_1}_{\nu 1}/J^{'r_1}_{\nu 1}$. The abbreviations $H^\rho_{\nu\kappa} = H^{(1)}_\nu(k_{\kappa\rho}\rho)$ and $J^\rho_{\nu\kappa} = J_\nu(k_{\kappa\rho}\rho)$ are Hankel and Bessel functions, respectively, of the first kind with an order ν and $k^2_{\kappa\rho} = \omega^2\mu_0\varepsilon_0\varepsilon_{r\kappa} - k_z^2$ for $\kappa = 1, 2, \ldots, K$. In the above expressions, the boundary condition on the tangential components of the electric field (E_z and E_ϕ) at $\rho = r_1$ have already been imposed.

As for the z components of the electric and magnetic fields due to a point source inside the substrate layers ($\kappa = 1, 2, \ldots, \kappa_\psi - 1$) for the ξth antenna placed at r_{κ_ψ} the expressions in each layer have the following form:

$$F_z^{feed,\xi}(\rho,\phi,z) = \frac{d\rho'}{8\pi}\sum_{\nu=-\infty}^{\infty} e^{i\nu\phi}\int_{-\infty}^{\infty} dk_z e^{ik_z z} \times$$

$$\begin{cases} \left(H^\rho_{\nu 1} - J^\rho_{\nu 1}\beta_1^\zeta\right) B^\zeta_{\nu 1} & r_1 \le \rho \le \ \rho' \\ \left(H^\rho_{\nu 1} - J^\rho_{\nu 1}\beta_1^\zeta\right) B^\zeta_{\nu 1} + \beta_1^{'\zeta} & \rho' \le \rho \le \ r_2 \\ \beta_\kappa^\zeta \beta_\kappa^{'\zeta} J^\rho_{\nu\kappa} + H^\rho_{\nu\kappa} B^\zeta_{\nu\kappa} + J^\rho_{\nu\kappa} B^{'\zeta}_{\nu\kappa} & r_\kappa \le \rho \le \ \rho' \\ \beta_\kappa^\zeta \beta_\kappa^{''\zeta} H^\rho_{\nu\kappa} + H^\rho_{\nu\kappa} B^\zeta_{\nu\kappa} + J^\rho_{\nu\kappa} B^{'\zeta}_{\nu\kappa} & \rho' \le \rho \le \ r_{\kappa+1} \\ \qquad \kappa = 2, \ldots, \kappa_\psi - 1, & \\ H^\rho_{\nu\kappa} B^\zeta_{\nu\kappa} + J^\rho_{\nu\kappa} B^{'\zeta}_{\nu\kappa} & r_\kappa \le \rho \le r_{\kappa+1} \\ \qquad \kappa = \kappa_\psi, \ldots, K-1, & \\ H^\rho_{\nu K} B^\zeta_{\nu K} & r_K \le \rho \end{cases} \quad (3)$$

where $F^{feed} = \{iE^{feed}, H^{feed}\}$, $\beta_1^{'e} = \frac{\alpha_\xi k_z k_{1\rho}}{\omega\varepsilon_1}(H^\rho_{\nu 1} J^{'\rho'}_{\nu 1} - H^{'\rho'}_{\nu 1} J^\rho_{\nu 1})$, $\beta_1^{'h} = \frac{\nu\alpha_\xi}{\rho'}(H^\rho_{\nu 1} J^{\rho'}_{\nu 1} - H^{\rho'}_{\nu 1} J^\rho_{\nu 1})$, $\beta^e_\kappa = \frac{\alpha_\xi k_z k_{\kappa\rho}}{\omega\varepsilon_\kappa}$, $\beta^h_\kappa = \frac{\nu\alpha_\xi}{\rho'}$, $\beta^{'e}_\kappa = H^{'\rho'}_{\nu\kappa}$, $\beta^{'h}_\kappa = H^{\rho'}_{\nu\kappa}$, $\beta^{''e}_\kappa = J^{'\rho'}_{\nu\kappa}$, $\beta^{''h}_\kappa = J^{\rho'}_{\nu\kappa}$, and $\alpha_\xi = I_{f\xi}e^{-i(\nu\phi_{f\xi} + k_z z_{f\xi})}$. $B^\zeta_{\nu\kappa}$ and $B^{'\zeta}_{\nu\kappa}$ are unknown coefficients of the harmonic order ν to be determined by the boundary conditions. The total electric and magnetic fields due to point sources for the structure with Ξ antennas are then the superposition of the fields:

$$F_z^{feed}(\rho,\phi,z) = \sum_{\xi=1}^{\Xi} F_z^{feed,\xi}(\rho,\phi,z) \quad (4)$$

From z components of the electric and magnetic fields, the ϕ and ρ components can easily be obtained. By imposing the boundary conditions of transverse electric and magnetic fields across all boundaries $\rho = r_2, r_3, \ldots, r_K$, the unknown coefficients can be obtained and the expressions for the transverse fields of $E^{patch}_{z,\phi}$ and $E^{feed}_{z,\phi}$ on all patch surfaces and can be written as follows [15], [19]:

$$\mathbf{E^{patch}} = \frac{1}{2\pi}\sum_{\nu=-\infty}^{\infty} e^{i\nu\phi}\int_{-\infty}^{\infty} dk_z e^{ik_z z}\mathbf{G}_\nu(k_z)\tilde{\mathbf{J}}_\nu(k_z) \quad (5)$$

$$\mathbf{E^{feed}} = \frac{1}{2\pi}\sum_{\nu=-\infty}^{\infty} e^{i\nu\phi}\int_{-\infty}^{\infty} dk_z e^{ik_z z}\frac{1}{4}\mathbf{S}_\nu(k_z) \quad (6)$$

with

$$\mathbf{S}_\nu(k_z) = \mathbf{T}_\nu(k_z)\mathbf{R}_\nu(k_z) + \mathbf{O}_\nu(k_z) \quad (7)$$

where the electric vectors $\mathbf{E} = \{\mathbf{E}^{patch}, \mathbf{E}^{feed}\}$, the vector of the patch surface current densities $\tilde{\mathbf{J}}_\nu(k_z)$, the Green matrix $\mathbf{G}_\nu(k_z)$, the matrix $\mathbf{T}_\nu(k_z)$ and the vectors $\mathbf{R}_\nu(k_z)$ and $\mathbf{O}_\nu(k_z)$ have the following form:

$$\mathbf{E} = (E_{\phi,1}(\cdot), \ldots, E_{\phi,\Psi}(\cdot), E_{z,1}(\cdot), \ldots, E_{z,\Psi}(\cdot))^T$$
$$\tilde{\mathbf{J}}_\nu(\cdot) = (\tilde{J}_{\phi\nu,1}(\cdot), \tilde{J}_{\phi\nu,\Psi}(\cdot), \ldots, \tilde{J}_{z\nu,1}(\cdot), \tilde{J}_{z\nu,\Psi}(\cdot))^T$$

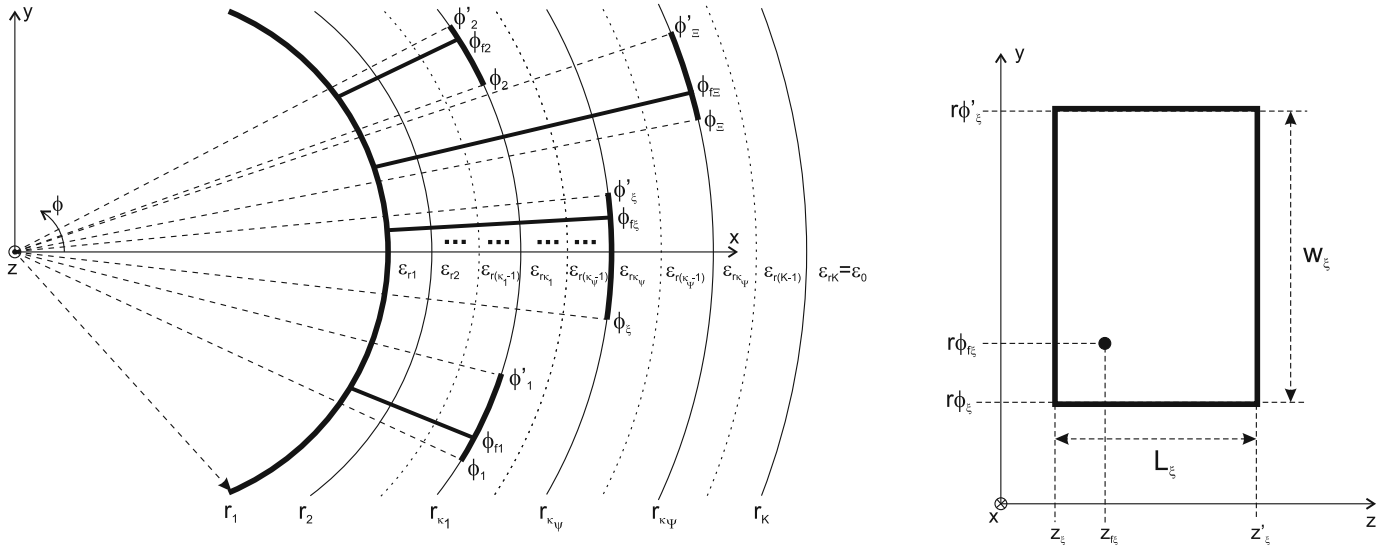

Fig. 1. The geometry of an investigated antenna structure - a probe-fed multi substrate and superstrate cylindrical–rectangular microstrip antennas

$$\mathbf{G}_\nu(\cdot) = \begin{bmatrix} \mathbf{G}_{\phi\phi,\nu}(\cdot) & \mathbf{G}_{\phi z,\nu}(\cdot) \\ \mathbf{G}_{z\phi,\nu}(\cdot) & \mathbf{G}_{zz,\nu}(\cdot) \end{bmatrix}$$

$$\mathbf{T}_\nu = \begin{bmatrix} \mathbf{T}_{ee,\nu} & \mathbf{T}_{eh,\nu} \\ \mathbf{T}_{he,\nu} & \mathbf{T}_{hh,\nu} \end{bmatrix}, \mathbf{R}_\nu = \begin{bmatrix} \mathbf{R}_{e,\nu} \\ \mathbf{R}_{h,\nu} \end{bmatrix}, \mathbf{O}_\nu = \begin{bmatrix} \mathbf{O}_{\phi,\nu} \\ \mathbf{O}_{z,\nu} \end{bmatrix}$$

where:

$$\mathbf{G}_{(\cdot),\nu} = \begin{bmatrix} G^{11}_{(\cdot),\nu} & \cdots & G^{1\Psi}_{(\cdot),\nu} \\ \vdots & \ddots & \vdots \\ G^{\Psi 1}_{(\cdot),\nu} & \cdots & G^{\Psi\Psi}_{(\cdot),\nu} \end{bmatrix}$$

$$\mathbf{T}_{(\cdot),\nu} = \begin{bmatrix} T^{11}_{(\cdot),\nu} & T'^{11}_{(\cdot),\nu} & \cdots & T^{1\Psi}_{(\cdot),\nu} & T'^{1\Psi}_{(\cdot),\nu} \\ \vdots & & & & \vdots \\ T^{\Psi 1}_{(\cdot),\nu} & T'^{\Psi 1}_{(\cdot),\nu} & \cdots & T^{\Psi\Psi}_{(\cdot),\nu} & T'^{\Psi\Psi}_{(\cdot),\nu} \end{bmatrix}$$

$$\mathbf{R}_{(\cdot),\nu} = \left(R^1_{(\cdot),\nu}, R'^1_{(\cdot),\nu}, \ldots, R^\Psi_{(\cdot),\nu}, R'^\Psi_{(\cdot),\nu}\right)^T$$

$$\mathbf{O}_{(\cdot),\nu} = (O^1_{(\cdot),\nu}, \ldots, O^{\Psi-1}_{(\cdot),\nu}, 0)^T$$

If the structure does not have any superstrates, (i.e., if there are patches placed on the layer $\rho = r_K$), matrix $\mathbf{T}_{(\cdot),\nu}$ does not have the last column and vector $\mathbf{R}_{(\cdot),\nu}$ does not have the last element.

The patch surface current densities in the spectral domain are defined as follows:

$$\begin{bmatrix} \tilde{J}_{\phi\nu}(k_z) \\ \tilde{J}_{z\nu}(k_z) \end{bmatrix} = \frac{1}{2\pi} \int_{-\pi}^{\pi} d\phi e^{-i\nu\phi} \int_{-\infty}^{\infty} dz e^{-ik_z z} \begin{bmatrix} J_\phi(\phi, z) \\ J_z(\phi, z) \end{bmatrix} \quad (8)$$

Matrix $\mathbf{G}_\nu(k_z)$ and vector $\mathbf{S}_\nu(k_z)$ can be obtained for any number of substrates and superstrates and any localization of patch antennas in the investigated structure, utilizing the straightforward formula presented in appendix A.

Summing the fields (5) and (6), we obtain the integral equation in the following form:

$$\sum_{\nu=-\infty}^{\infty} e^{i\nu\phi} \int_{-\infty}^{\infty} dk_z e^{ik_z z} \mathbf{G}_\nu(k_z) \tilde{\mathbf{J}}_\nu(k_z) = = -\sum_{\nu=-\infty}^{\infty} e^{i\nu\phi} \int_{-\infty}^{\infty} dk_z e^{ik_z z} \frac{1}{4} \mathbf{S}_\nu(k_z) \quad (9)$$

Note that due to the orthogonality properties of eigenfunctions $e^{i\nu\phi}$ the above problem can be solved for each eigenvalue ν separately. The integral equation (9) is solved using Galerkin's moment method. Following Galerkin's procedure, the surface current densities on the patch are expanded in terms of a linear combination of known basis functions:

$$\vec{J}(\phi, z) = \sum_{n=1}^{N_\xi} I_n^{(\xi)} \left(J^{(\xi)}_{\phi n}(\phi, z) \vec{i}_\phi + J^{(\xi)}_{zn}(\phi, z) \vec{i}_z \right) \quad (10)$$

where $I_n^{(\xi)}$ denotes unknown coefficients for the nth mode of the basis functions for the ξth patch. The most common choice of the basis functions is the cavity-model function with or without the edge-singularity condition for the tangential component of the surface current at the patch edge. The basis functions without the edge-singularity condition has the following form:

$$J^{(\xi)}_{\phi n}(\phi, z) = \frac{n_\phi \pi}{k_c^2 W_\xi} \sin \frac{n_\phi \pi(\phi - \phi_\xi)}{\phi'_\xi - \phi_\xi} \cos \frac{n_z \pi(z - z_\xi)}{z'_\xi - z_\xi} \quad (11)$$

$$J^{(\xi)}_{zn}(\phi, z) = \frac{n_z \pi}{k_c^2 L_\xi} \cos \frac{n_\phi \pi(\phi - \phi_\xi)}{\phi'_\xi - \phi_\xi} \sin \frac{n_z \pi(z - z_\xi)}{z'_\xi - z_\xi} \quad (12)$$

with $k_c = \sqrt{\left(\frac{n_\phi \pi}{W_\xi}\right)^2 + \left(\frac{n_z \pi}{L_\xi}\right)^2}$ where $n_\phi, n_z = 0, 1, \ldots, \infty$ and their combination denotes the mode number of the basis function. The spectral amplitudes of the current distribution

are calculated from:

$$\tilde{J}_u(k_z) = \frac{1}{2\pi}\int\limits_{\phi_\xi}^{\phi'_\xi} d\phi e^{-iu\phi}\int\limits_{z_\xi}^{z'_\xi} dz e^{-ik_z z} J(\phi, z) \tag{13}$$

Substituting the calculated spectral components of the current distributions into (9) and then using the chosen basis functions as testing functions and integrating the obtained equation over the patch area, the following matrix equation is obtained:

$$(\mathbf{Z}_{\phi\phi} + \mathbf{Z}_{\phi z} + \mathbf{Z}_{z\phi} + \mathbf{Z}_{zz})\,\mathbf{I} = (\mathbf{V}_\phi + \mathbf{V}_z) \tag{14}$$

where $\mathbf{I} = [I_1^{(1)}, \ldots, I_{N_1}^{(1)}, \ldots, I_1^{(\Xi)}, \ldots, I_{N_\Xi}^{(\Xi)}]^T$ (N_ξ - number of modes for the ξth patch antenna). When the patch antennas are placed on the Ψ layers and when on each layer there are Ξ_ψ ($\psi = 1, \ldots, \Psi$) patches, the matrix $\mathbf{Z}_{(\cdot)}$ and vector $\mathbf{V}_{(\cdot)}$ are constructed as follows:

$$\mathbf{Z}_{(\cdot)} = \begin{bmatrix} \mathbf{Z}_{(\cdot)}^{11} & \cdots & \mathbf{Z}_{(\cdot)}^{1\Psi} \\ \vdots & \ddots & \vdots \\ \mathbf{Z}_{(\cdot)}^{\Psi 1} & \cdots & \mathbf{Z}_{(\cdot)}^{\Psi\Psi} \end{bmatrix}, \qquad \mathbf{V}_{(\cdot)} = \begin{bmatrix} \mathbf{V}_{(\cdot)}^{1} \\ \vdots \\ \mathbf{V}_{(\cdot)}^{\Psi} \end{bmatrix} \tag{15}$$

The dimensions of each submatrix $\mathbf{Z}_{(\cdot)}^{pq}$ and the length of the subvector $\mathbf{V}_{(\cdot)}^{p}$ ($p, q = 1, \ldots, \Psi$) depend on the number of patch antennas located on each layer. If we assume that the surface current density for ξth patch antenna has a different number of expansion terms, the total number of considered modes for the entire structure equals N, defined as follows:

$$N = \sum_{\psi=1}^{\Psi} M_\psi, \qquad M_\psi = \sum_{\xi=1}^{\Xi_\psi} N_\xi^\psi \tag{16}$$

where M_ψ is a total number of modes on ψth layer and N_ξ^ψ is a number of surface current density expansion terms for the ξth antenna on the ψth layer, with Ξ_ψ being a number of antennas on the ψth layer. With this assumption, the submatrix $\mathbf{Z}_{(\cdot)}^{pq}$ and the subvector $\mathbf{V}_{(\cdot)}^{p}$ ($p, q = 1, \ldots, \Psi$) are of dimensions $M_p \times M_q$ and $M_p \times 1$, respectively, and have the form:

$$\mathbf{Z}_{(\cdot)}^{pq} = \begin{bmatrix} \mathbf{Z}_{(\cdot)}^{pq,11} & \cdots & \mathbf{Z}_{(\cdot)}^{pq,1\Xi_q} \\ \vdots & & \vdots \\ \mathbf{Z}_{(\cdot)}^{pq,\Xi_p 1} & \cdots & \mathbf{Z}_{(\cdot)}^{pq,\Xi_p\Xi_q} \end{bmatrix}, \quad \mathbf{V}_{(\cdot)}^{p} = \begin{bmatrix} \mathbf{V}_{(\cdot)}^{p,1} \\ \vdots \\ \mathbf{V}_{(\cdot)}^{p,\Xi_p} \end{bmatrix} \tag{17}$$

The terms of the submatrices $\mathbf{Z}_{(\cdot)}^{pq,st}$ and subvectors $\mathbf{V}_{(\cdot)}^{p,s}$ ($s = 1, \ldots, \Xi_p$, $t = 1, \ldots, \Xi_q$) are defined as follows:

$$(\mathbf{Z}_{x,y}^{pq,st})_{vw} = \int\limits_{-\infty}^{\infty} dk_z \sum_{u=-\infty}^{\infty} \tilde{J}_{xv,-u}^{p,s}(-k_z) G_{xy,u}^{pq}(k_z) \tilde{J}_{yw,u}^{q,t}(k_z) \tag{18}$$

$$(\mathbf{V}_{(\cdot)}^{p,s})_v = \int\limits_{-\infty}^{\infty} dk_z \sum_{u=-\infty}^{\infty} \tilde{J}_{xv,-u}^{p,s}(-k_z) \mathbf{S}_u^p(k_z) \tag{19}$$

where $x, y = (\phi, z)$ $\mathbf{S}_u^p(\cdot)$ is pth element of vector $\mathbf{S}_u(\cdot)$ defined in (7). Note that the elements of matrix $\mathbf{Z}$ in (14) allows the determination of the coupling between the patch antennas.

The procedure for constructing the Green matrix $\mathbf{G}$ and the vector $\mathbf{S}$ is presented in appendix A.

III. Impedance of the Patch Antenna and the Radiation Pattern

In order to calculate the impedance Z_D, of a single probe-fed patch antenna placed on layer κ' in the structure, we can use the following formula [15]:

$$Z_D = -\frac{1}{2\pi I_f}\sum_{\kappa=1}^{\kappa'-1}\int\limits_{r_\kappa}^{r_{\kappa+1}} d\rho \sum_{\nu=-\infty}^{\infty} e^{i\nu\phi_f} \times \int\limits_{-\infty}^{\infty} dk_z e^{ik_z z_f} \mathbf{G}_\nu^{'\kappa}(k_z)\tilde{\mathbf{J}}_\nu(k_z) \tag{20}$$

with vector $\mathbf{G}_\nu^{'\kappa}(\cdot)$ defined in appendix B.

The far-zone radiated fields in the spherical coordinates are given by [15]:

$$\begin{bmatrix} E_\theta \\ E_\phi \end{bmatrix} \cong \frac{1}{\sin\theta}\begin{bmatrix} -1 & 0 \\ 0 & \sqrt{\frac{\mu_0}{\varepsilon_0}} \end{bmatrix} \frac{-ie^{ik_0 r}}{\pi r} \sum_{\nu=-\infty}^{\infty} e^{i\nu\phi} \times \frac{(-i)^\nu}{H_\nu^{(1)}(k_0 r_K \sin\theta)} \mathbf{\Gamma}_\nu(k_0\cos\theta)\tilde{\mathbf{J}}_\nu(k_0\cos\theta) \tag{21}$$

where the elements of matrix $\mathbf{\Gamma}_\nu$ depend on the location of the patch antennas in the structure. Matrix $\mathbf{\Gamma}_\nu$ is defined in appendix B.

IV. Results

In this section the numerical results of several chosen antenna configuration are presented. The calculations of the input impedances of single antenna configurations and the radiation patterns for chosen single antennas and antenna arrays are performed and the obtained results are compared with those presented in the literature and our own measurements.

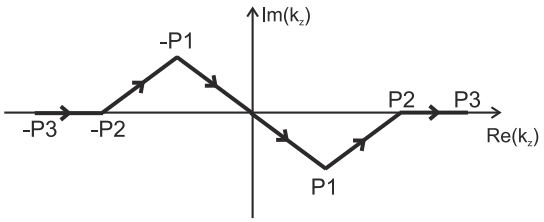

Fig. 2. Deformed integration path.

Along the original path of integration, branch-point singularities and pole singularities are encountered [30], [31], which makes the integrals (18) and (19) not-integrable along the real axis on the complex k_z plane. To avoid these branch-point singularities, a deformed path, proposed in [31] and shown in Fig. 2, is chosen. The points $P1$, $P2$ and $P3$ are defined as follows: $P1 = k_0(1 - iT_1)$, $P2 = k_0\sqrt{1+T_2^2}$, $P3 = k_0\sqrt{1+T_3^2}$, where parameters T_1, T_2, and T_3 need to be chosen properly to obtain accurate results. From the performed calculations and according to [31], for the presented examples the values of these parameters are as follows: $T_1 = (0.2 - 0.5)$, $T_2 = (20 - 30)$, and $T_3 = (1.1 - 5)T_2$. For the presented examples of input impedance calculation, it was sufficient to select 30 terms for the convergence of u-series of (18) and (19). In the case of radiation pattern calculation 10

terms were found to be sufficient for the convergence of these series.

The first example is a single patch structure proposed in [32]. The antenna is situated on a single dielectric substrate. The schematic representation of the structure with its dimensions is illustrated in Fig. 3 along with the calculated real and imaginary parts of the antenna input impedance versus frequency. The obtained results are compared with calculations presented in [19], [12] and measurement results from [32], and good agreement is achieved, which validates the proposed approach.

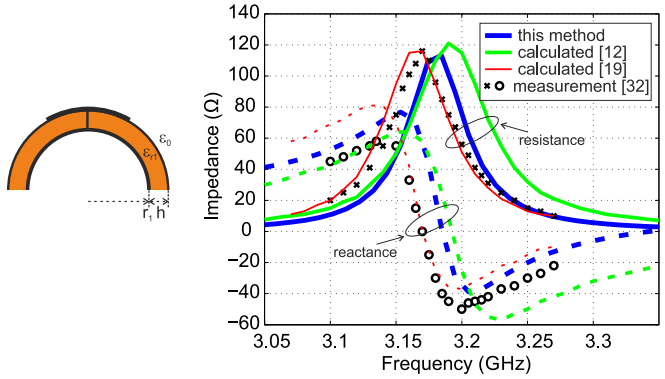

Fig. 3. The geometry of the antenna and calculated input impedance of the HE_{01} mode versus the frequency for the antenna with the dimensions: $r_1 = 5$ cm; $\varepsilon_r = 2.32$; $h = 0.795$ mm; $L = 3$ cm; $W = 4$ cm; $\phi_f = 0$, $z_f = 1$ cm.

Next, the influence of the superstrate thickness on the antenna input impedance is investigated. The dimensions of the structure are the same as in the first example, and a superstrate layer with a different thickness t is assumed. The calculated real and imaginary parts of the antenna input impedance versus the frequency with the structure geometry are presented in Fig. 4. The existence of the superstrate layer lowers the resonant frequency of the antenna. The results are consistent with those presented in [19].

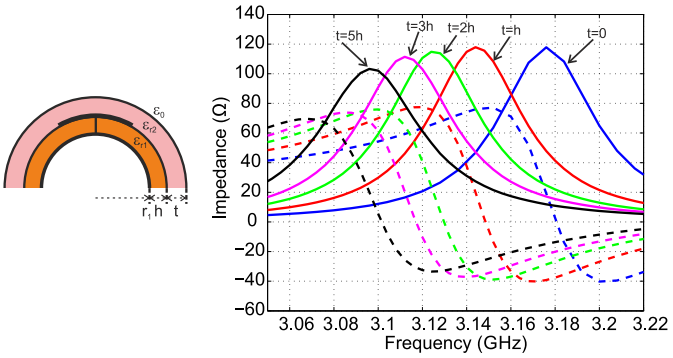

Fig. 4. The geometry of the antenna and calculated input impedances of the HE_{01} mode versus the frequency for the different values of the superstrate thickness. Structure dimensions: $r_1 = 5$ cm, $\varepsilon_{r1} = 2.32$, $\varepsilon_{r2} = 2.32$,$h = 0.795$ mm, $L = 3$ cm, $W = 4$ cm; probe feed $\phi_f = 0$, $z_f = 1$ cm. Solid line - resistance, dashed line - reactance.

The third example is a single patch antenna situated on a dielectric substrate and an air gap between the substrate and the ground cylinder with a thickness s. The input impedance characteristics for different air gap thicknesses s are presented in Fig. 5. The obtained results are compared with those presented in [17]. As the considered structure was investigated in [17] as the resonance problem, only the resonance frequencies are marked in Fig. 5. From the obtained results, it is seen that the resonant frequency increases as the air gap thickness is increased, until the thickness reaches a value of 5 mm, for the considered case, when the resonant frequency starts to decrease. This is due to the effective permittivity of the region under the patch, which lowers with the increasing thickness of the air gap. With high values of the air gap thickness, the effective permittivity of the region varies slightly and the thickness of the region under the patch starts to dominate the effect, which reduces the resonant frequency. The obtained results agree well with those presented in [17]. It can be seen that the half-power bandwidth of the structure increases considerably due to the existence of an air gap which is also consistent with the calculations presented in [17].

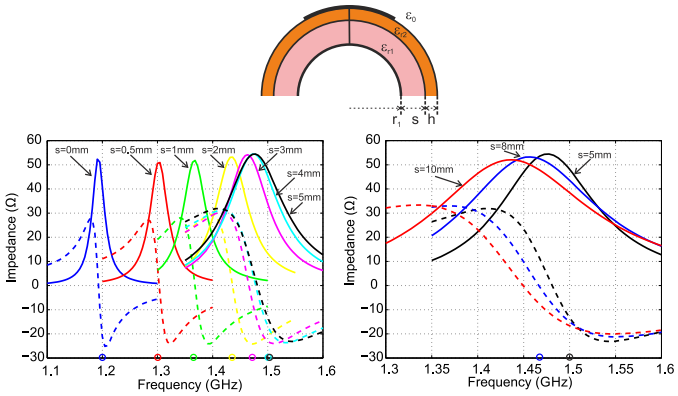

Fig. 5. The geometry of the antenna and calculated input impedances of the HE_{01} mode versus the frequency for different air gaps ($\varepsilon_{r1} = 1$) of thickness s; ground cylinder radius $r_1 = 20$ cm; substrate permittivity $\varepsilon_{r2} = 2.32$ and thickness $h = 2.4$ mm; antenna dimensions: $L = 8$ cm, $W = 16.8$ cm; probe feed $\phi_f = 0$, $z_f = 2$ cm. Solid line - resistance, dashed line - reactance.

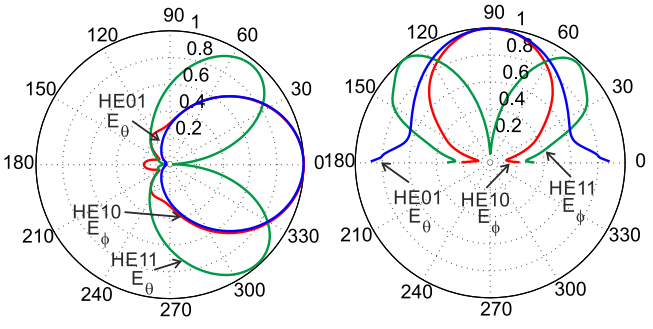

Fig. 6. Calculated radiation pattern around the resonance of the rectangular patch on a single substrate $\varepsilon_{r1} = 2.3$ for the HE_{10} mode ($|E_\phi|$) and the HE_{01} mode ($|E_\theta|$) at $f = 1.2$ GHz, and the HE_{11} mode at $f = 1.7$ GHz. Structure dimensions: $r_1 = 10$ cm, $h = 2$ mm. $L = W = 8$ cm. (a) Radiation pattern versus ϕ, in the plane $\theta = 90°$. (b) Radiation pattern versus θ in the plane $\phi = 0°$.

Next, the radiation patterns for single and multiple antenna configurations are investigated. Fig. 6 shows the radiation pattern around the resonance of a single rectangular patch

on a single substrate, as proposed in [15], for the HE_{10} and HE_{01} modes at $f = 1.2$ GHz and the HE_{11} mode at $f = 1.7$ GHz. The obtained results agree well with those presented in [15], except for the HE_{01} mode E_θ. Note, that the results calculated for the HE_{01} mode strongly depend on the calculation of the spectral amplitude of the current distribution from (13) for the case where $n_\phi = 0$. From the performed calculations, we found out that the results presented in [15] were obtained by wrongly calculating the spectral amplitude of the current distribution for the case where $n_z = 0$ and $n_\phi = 0$. Substituting (11) and (12) to (13), the values of these spectral amplitudes in this case take the form:

$$\tilde{J}_{u=0,\phi(n_\phi=0,n_z)}(k_z) = 0$$

$$\tilde{J}_{u=0,z(n_\phi=0,n_z)}(k_z) = \frac{1}{2\pi}\int_{\phi_\xi}^{\phi'_\xi} d\phi \int_{z_\xi}^{z'_\xi} dz e^{-ik_z z} \times \frac{n_z\pi}{k_c^2 L_\xi} \sin\frac{n_z\pi(z-z_\xi)}{z'_\xi - z_\xi}$$

If one assumes that both of these spectral amplitudes in the considered case equal 0, the results will be consistent with inaccurate patterns presented in [15]. The authors in [13] have also analyzed this example comparing their results with those presented in [15], however, they have omitted the case for the HE_{01} mode calculated versus ϕ in the plane $\theta = 90°$.

To additionally check the validity of the proposed procedure, single and double antenna configurations were manufactured and measured, and the obtained results were compared with the calculated ones. The photo of the manufactured configuration is presented in Fig. 7. The antennas were realized on the Taconic RF-35 substrate.

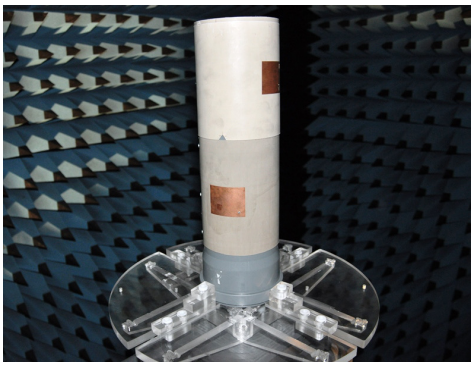

Fig. 7. Photograph of the manufactured antenna configuration in the anechoic chamber.

The calculated and measured input impedances of a single antenna configuration for different substrate thicknesses are illustrated in Fig. 8. Next, the superstrate of different thickness t was added to the antenna and the obtained results are depicted in Fig. 9. However, the manufactured antennas produce lower resistance values than the calculated ones the satisfactory agreement between results is achieved.

The radiation patterns of the antenna configurations were also measured. Fig. 10 illustrates the radiation patterns around the resonance of a single rectangular patch on a single

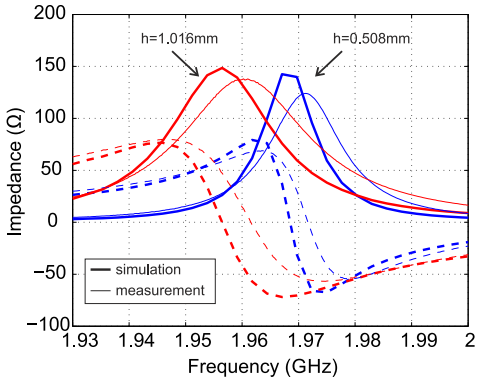

Fig. 8. Calculated and measured input impedances of the HE_{01} mode versus the frequency for the single antenna structure with the dimensions: $r_1 = 5.5$ cm, $\varepsilon_{r1} = 3.57$, $h = (0.508, 1.016)$ mm, $L = 4$ cm, $W = 5$ cm; probe feed $\phi_f r_2 = 4.22$ cm, $z_f = 3.37$ cm. Solid line - resistance, dashed line - reactance.

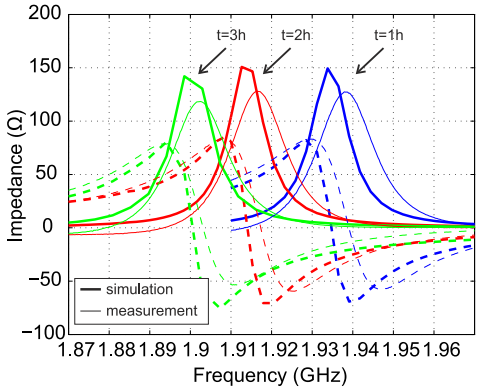

Fig. 9. Calculated and measured input impedances of the HE_{01} mode versus the frequency for different superstrate thicknesses $t = (1h, 2h, 3h)$ for the structure with the dimensions: $r_1 = 5.5$ cm, $\varepsilon_{r1} = 3.57$, $\varepsilon_{r2} = 10.2$, $h = 0.508$ mm, $L = 4$ cm, $W = 5$ cm; probe feed $\phi_f r_2 = 4.22$ cm, $z_f = 3.37$ cm. Solid line - resistance, dashed line - reactance.

substrate for the HE_{10} mode at $f = 1.58$ GHz and the HE_{01} mode at $f = 1.98$ GHz. Fig. 11 shows the radiation patterns around the resonances, as in Fig. 10 for a double patch configuration on a single substrate. The antennas are located on the same z level and are placed symmetrically around the x axis (symmetrically, around $\phi = 0$) with a circumferential distance 15 cm between their centers. In the next example, the antennas were located on different substrate layers and are schematically presented in Fig. 12. Both layers are made with the same dielectric material. Adding a superstrate layer to one antenna and doubling the thickness of the substrate layer in the other slightly lowered their resonance frequencies. However, for both antennas the new resonance frequencies - and in consequence the matching frequency - were the same, which allowed the measurement of the manufactured configuration. The obtained results are presented in Fig. 12.

As can be seen from the obtained results a satisfactory agreement between the results was obtained. The discrepancies may result from the manufacturing process of antennas and the fact that the dielectric material did not surround the entire cylinder, creating a gap on one side of the structure.

As the last example the array of rectangular patches along

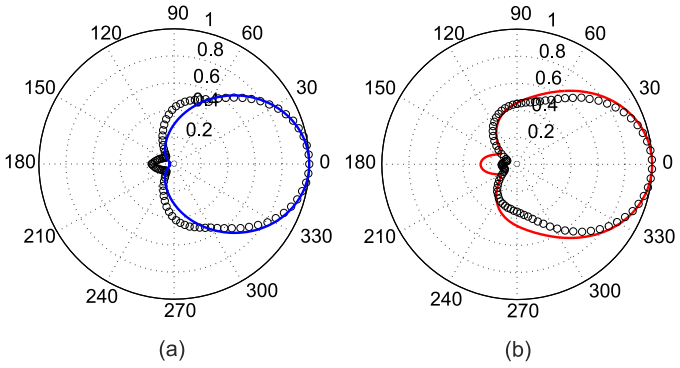

Fig. 10. The calculated and measured radiation patterns around the resonance of the rectangular patch on a single substrate $\varepsilon_{r1} = 3.57$ for: (a) the HE_{10} mode ($|E_\phi|$) at $f = 1.58$ GHz; (b) the HE_{01} mode ($|E_\theta|$) at $f = 1.98$ GHz. Structure dimensions: $r_1 = 5.5$ cm, $h = 0.508$ mm. $L = 4$ cm, $W = 5$ cm. Radiation pattern versus ϕ, in the plane $\theta = 90°$. Solid line - calculation, circle line - measurement.

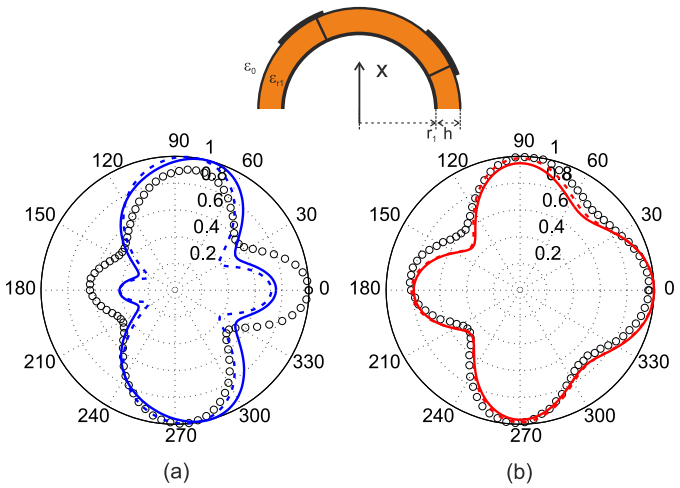

Fig. 11. The calculated and measured radiation patterns around the resonance of two rectangular patches on a single substrate $\varepsilon_{r1} = 3.57$ for: (a) the HE_{10} mode ($|E_\phi|$) at $f = 1.58$ GHz; (b) the HE_{01} mode ($|E_\theta|$) at $f = 1.98$ GHz. Structure dimensions: $r_1 = 5.5$ cm, $h = 0.508$ mm. $L_1 = L_2 = 4$ cm, $W_1 = W_2 = 5$ cm. The patches are located on the same z level and the circumferential distance between their centers is 15 cm (symmetrically around the x axis). Radiation pattern versus ϕ, in the plane $\theta = 90°$. Solid line - this method, dashed line - HFSS, circle line - measurement.

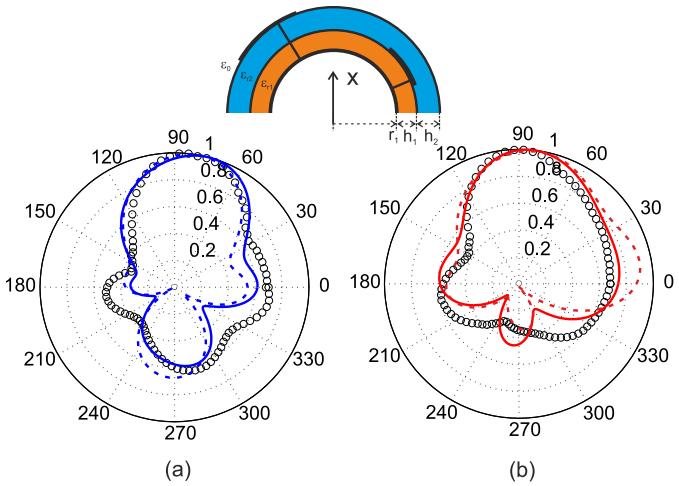

Fig. 12. The calculated and measured radiation patterns around the resonance of two rectangular patches located on different layers of the substrate $\varepsilon_{r1} = \varepsilon_{r2} = 3.57$ for: (a) the HE_{10} mode ($|E_\phi|$) at $f = 1.56$ GHz; (b) the HE_{01} mode ($|E_\theta|$) at $f = 1.97$ GHz. Structure dimensions: $r_1 = 5.5$ cm, $h_1 = h_2 = 0.508$ mm. $L_1 = L_2 = 4$ cm, $W_1 = W_2 = 5$ cm. The patches are located on the same z level and the circumferential distance between their centers is 15 cm (symmetrically around the x axis). Radiation pattern versus ϕ, in the plane $\theta = 90°$. Solid line - this method, dashed line - HFSS, circle line - measurement.

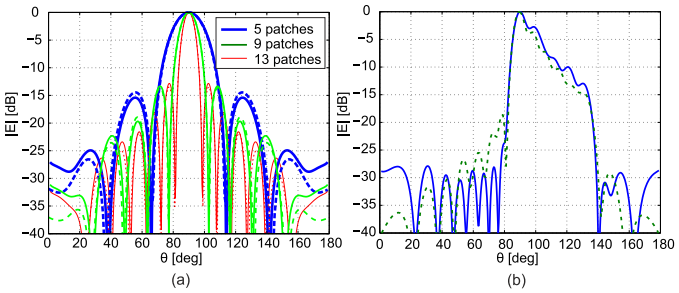

Fig. 13. The calculated radiation patterns of the HE_{10} mode ($|E_\phi|$) for the arrays of rectangular patches $L = W = 5$ cm, located on a single layer of the substrate arranged along the axis of the cylinder $r_1 = 5$ cm (for the same ϕ angle) with distance $\lambda/2$: (a) arrays of 5, 9 and 13 patches located on substrate $\varepsilon_{r1} = 3.5$, $h_1 = 0.508$ mm at $f = 1.5$ GHz with the same excitation; (b) array of 17 patches located on substrate $\varepsilon_{r1} = 3.5$, $h_1 = 2.5$ mm at $f = 1$ GHz with the excitations form [33]. Solid line - this method, dashed line - HFSS.

z axis is investigated. The radiation patterns of the equidistant antenna arrays of 5, 9 and 13 patches with the same excitation were calculated and presented in Fig. 13(a). The more antennas in the array the narrower main lobe of the pattern. The results well agree with the calculation of linear array of planar patches. The equidistant array of 17 patches producing cosecant beam extending from $\theta = 90°$ to $\theta = 135°$ (with excitations form [33]) is calculated and its radiation pattern is presented in Fig. 13(b). The results were compared with those obtained from HFSS commercial simulator and good agreement is achieved.

V. Conclusion

The unified procedure for creating proper matrices for a multi-layer and multi-patch configuration of the antenna structure composed of probe-fed rectangular microstrip antennas mounted on a cylindrical body was proposed. A full-wave analysis and a moment-method calculation were employed. Calculating the proper matrices for the antenna with modified structure (e.g., additional superstrate cover or an air gap in the substrate layer) can be performed, with proposed procedure, automatically without the need to perform additional mathematical transformations. The input impedances and radiation patterns for several antenna examples were derived. The obtained results were verified by comparing them with results from the literature and our own measurements of manufactured prototypes, and good agreement was achieved.

Appendix A
Matrix G and vector S for multi-layer and multi-patch antenna configuration

Here, we describe a procedure for creating a Green matrix $\mathbf{G}$ defined in (5) for the electric field due to the current distribution on the patches, and vector $\mathbf{S}$ defined in (6) for

the electric field due to probe currents with the patches being absent, for arbitrary number of substrates and superstrates and arbitrary localization of antennas.

A. Creating the G matrix

For the structure presented in Fig. 1 composed of $K-1$ dielectric layers, each with a relative permittivity $\varepsilon_{r\kappa}$ ($\kappa = 1,2,\ldots,K-1$) and a free space on the outside of the structure $\varepsilon_{rK}=1$, there are $K-1$ interfaces ($\rho = r_2, r_3, \ldots, r_K$), where the boundary conditions between the tangential components of electric and magnetic fields need to be satisfied. Taking the field expressions in (2), the boundary condition on the metallic surface at $\rho = r_1$ is already imposed.

For the general case described above, the procedure can be outlined as follows:

1) Write the boundary conditions for the tangential components $\tilde{E}_z^{\kappa}$, $\tilde{E}_\phi^{\kappa}$, $\tilde{H}_z^{\kappa}$ and $\tilde{H}_\phi^{\kappa}$ in the spectral domain at each interface in the form of a set of equations:

$$\begin{aligned}
\tilde{E}^1_{(z,\phi)}(\rho=r_2) &- \tilde{E}^2_{(z,\phi)}(\rho=r_2)=0\\
\tilde{H}^1_{(z,\phi)}(\rho=r_2) &- \tilde{H}^2_{(z,\phi)}(\rho=r_2)=0\\
&\vdots\\
\tilde{E}^{\kappa_\psi-1}_{(z,\phi)}(\rho=r_{\kappa_\psi}) &- \tilde{E}^{\kappa_\psi}_{(z,\phi)}(\rho=r_{\kappa_\psi})=0\\
\tilde{H}^{\kappa_\psi-1}_{(z,\phi)}(\rho=r_{\kappa_\psi}) &- \tilde{H}^{\kappa_\psi}_{(z,\phi)}(\rho=r_{\kappa_\psi})=\pm\tilde{J}^{\psi}_{(\phi,z)}(k_z)\\
&\vdots\\
\tilde{E}^{K-1}_{(z,\phi)}(\rho=r_K) &- \tilde{E}^{K}_{(z,\phi)}(\rho=r_K)=0\\
\tilde{H}^{K-1}_{(z,\phi)}(\rho=r_K) &- \tilde{H}^{K}_{(z,\phi)}(\rho=r_K)=0
\end{aligned}$$

2) Rewrite the set of equations in matrix form, which for a chosen number ν takes the following form:

$$\mathbf{X}_\nu \mathbf{A}_\nu = \mathbf{F}_\nu \tag{22}$$

where $\mathbf{X}_\nu$ is a square matrix of dimension $4(K-1)$, the elements of which are the expressions standing next to unknown coefficients. $\mathbf{A}_\nu$ is a vector of length $4(K-1)$:

$$\mathbf{A}_\nu = \Big[A^e_{\nu 1}, A^h_{\nu 1}, A^e_{\nu 2}, A^h_{\nu 2}, A'^e_{\nu 2}, A'^h_{\nu 2}, \ldots, A^e_{\nu k_\psi}, A^h_{\nu k_\psi}, A'^e_{\nu k_\psi}, A'^h_{\nu k_\psi}, \ldots, A^e_{\nu K}, A^h_{\nu K}\Big]^T$$

$\mathbf{F}_\nu$ is a vector of length $4(K-1)$ of the following form:

$$\mathbf{F}_\nu = \Big[0,\ldots,\tilde{J}^1_{\phi\nu}(k_z), -\tilde{J}^1_{z\nu}(k_z),\ldots, \tilde{J}^\psi_{\phi\nu}(k_z), -\tilde{J}^\psi_{z\nu}(k_z),\ldots,\tilde{J}^\Psi_{\phi\nu}(k_z), -\tilde{J}^\Psi_{z\nu}(k_z),\ldots,0\Big]^T$$

where elements $\tilde{J}^\psi_{\phi\nu}(k_z)$ and $-\tilde{J}^\psi_{z\nu}(k_z)$ for $\psi = 1,\ldots,\Psi$ are located in the $4(\kappa_\psi-1)-1$ and $4(\kappa_\psi-1)$ positions, respectively.

3) In the next step, the matrix relation between the 2Ψ spectral-domain patch surface current densities and the 2Ψ chosen field amplitudes needs to be obtained. It is possible to pick any arbitrary amplitudes. Keeping in mind that the aim of the analysis is to find the electric field on the patch the best choice is to pick the amplitudes of the fields in regions located above or below the patches. Let us choose Ψ pairs of amplitudes $(A^e_{\nu\kappa_\psi}, A^h_{\nu\kappa_\psi})$ of the field in regions κ_ψ (above the patches). With this assumption, we rearrange the matrix equation (22) so that the chosen amplitudes are moved to the top of the amplitude vector, and the discontinuity equations with current densities are written first. The resultant matrix equation has the following form:

$$\begin{bmatrix} \mathbf{X'}_{1,\nu} & \mathbf{X'}_{2,\nu} \\ \mathbf{X'}_{3,\nu} & \mathbf{X'}_{4,\nu} \end{bmatrix} \begin{bmatrix} \mathbf{A}_{c\nu} \\ \mathbf{A}_{r\nu} \end{bmatrix} = \begin{bmatrix} \tilde{\mathbf{J}}_\nu \\ \mathbf{0} \end{bmatrix} \tag{23}$$

which can be easily rewritten into two separate matrix equations, as follows:

$$\mathbf{X'}_{1,\nu}\mathbf{A}_{c\nu} + \mathbf{X'}_{2,\nu}\mathbf{A}_{r\nu} = \tilde{\mathbf{J}}_\nu \tag{24}$$

$$\mathbf{X'}_{3,\nu}\mathbf{A}_{c\nu} + \mathbf{X'}_{4,\nu}\mathbf{A}_{r\nu} = \mathbf{0} \tag{25}$$

where the matrices $\mathbf{X'}_{j\nu}$ ($j=1,\ldots,4$) are composed from matrix $\mathbf{X}_\nu$ by rearranging its rows and columns, and are of the dimensions: $\mathbf{X'}_{1\nu}$ - $(2\Psi\times 2\Psi)$, $\mathbf{X'}_{2\Psi\nu}$ - $(2\times(4(K-1)-2\Psi))$, $\mathbf{X'}_{3\nu}$ - $((4(K-1)-2\Psi)\times 2\Psi)$ and $\mathbf{X'}_{4\nu}$ - $((4(K-1)-2\Psi)\times(4(K-1)-2\Psi))$. Vector $\mathbf{A}_{c\nu}$ contains the chosen amplitudes from the κ_ψ regions $\mathbf{A}_{c\nu} = \left[A^e_{\nu\kappa_1}, A^h_{\nu\kappa_1}, \ldots, A^e_{\nu\kappa_\Psi}, A^h_{\nu\kappa_\Psi}\right]^T$ and vector $\mathbf{A}_{r\nu}$ contains all the other amplitudes. The current densities vector is arranged as:

$$\tilde{\mathbf{J}}_\nu = \left[\tilde{J}^1_{\phi\nu}(k_z), -\tilde{J}^1_{z\nu}(k_z), \ldots, \tilde{J}^\Psi_{\phi\nu}(k_z), -\tilde{J}^\Psi_{z\nu}(k_z)\right]^T$$

and vector $\mathbf{0}$ is a zero vector of length $(4(K-1)-2\Psi)$.

4) From (25), the relation between the coefficients $\mathbf{A}_{r\nu}$ and $\mathbf{A}_{c\nu}$ is obtained:

$$\mathbf{A}_{r\nu} = -\mathbf{X'}^{-1}_{4,\nu}\mathbf{X'}_{3,\nu}\mathbf{A}_{c\nu} = \mathbf{X'}_{43,\nu}\mathbf{A}_{c\nu} \tag{26}$$

where $\mathbf{X'}_{43,\nu}$ is a $((4(K-1)-2\Psi)\times 2\Psi)$ matrix. Substituting (26) to (24) the following relation is derived:

$$\mathbf{A}_{c\nu} = \left(\mathbf{X'}_{1,\nu} + \mathbf{X'}_{2,\nu}\mathbf{X'}_{43,\nu}\right)^{-1}\tilde{\mathbf{J}}_\nu = \mathbf{X''}_\nu{}^{-1}\tilde{\mathbf{J}}_\nu \tag{27}$$

5) In order to relate the spectral-domain transverse components of the electric fields on the patches (in regions κ_ψ) and the patch surface current densities, the rest of the unknown coefficients of the fields in regions κ_ψ $(A'^e_{\nu\kappa_\psi}, A'^h_{\nu\kappa_\psi})$ need to be related to the chosen coefficients. From vector $\mathbf{A}_{r\nu}$ and matrix $\mathbf{X'}_{43,\nu}$, we can select rows related to the coefficients $A'^e_{\nu\kappa_\psi}$ and $A'^h_{\nu\kappa_\psi}$, and based on (26) we obtain the following relation:

$$\mathbf{A}_{c2\nu} = \mathbf{X''}_{43,\nu}\mathbf{A}_{c\nu} \tag{28}$$

where $\mathbf{A}_{c2\nu} = \left[A'^e_{\nu\kappa_1}, A'^h_{\nu\kappa_1}, \ldots, A'^e_{\nu\kappa_\Psi}, A'^h_{\nu\kappa_\Psi}\right]^T$ and $\mathbf{X''_{43,\nu}}$ is a $2\Psi\times 2\Psi$ matrix, which is composed from the $\mathbf{X'_{43,\nu}}$ matrix by selecting rows $(4(\kappa_\psi-1)-1)$ and $(4(\kappa_\psi-1))$.

6) The relation between the spectral-domain transverse components of the electric field on the patch (in region κ) and the patch surface current densities can be written by the following matrix equation:

$$\begin{aligned}
\begin{bmatrix} \tilde{\mathbf{E}}^{patch}_{\phi\nu}(k_z) \\ \tilde{\mathbf{E}}^{patch}_{z\nu}(k_z) \end{bmatrix} &= \begin{bmatrix} \mathbf{Y_{1}}_\nu & \mathbf{Y_{2}}_\nu \end{bmatrix} \begin{bmatrix} \mathbf{A}_{c\nu} \\ \mathbf{A}_{c2\nu} \end{bmatrix} = \\
&= \left(\mathbf{Y_{1}}_\nu + \mathbf{Y_{2}}_\nu\mathbf{X''_{43,\nu}}\right)\mathbf{A}_{c\nu} = \\
&= \left(\mathbf{Y_{1}}_\nu + \mathbf{Y_{2}}_\nu\mathbf{X''_{43,\nu}}\right)\mathbf{X''}_\nu{}^{-1}\tilde{\mathbf{J}}_\nu
\end{aligned} \tag{29}$$

where $\mathbf{Y_{1}}_{\nu}$ and $\mathbf{Y_{2}}_{\nu}$ are $2\Psi \times 2\Psi$ matrices, the elements of which are the expressions standing next to the unknown coefficients in the κ_ψ regions.

The resultant $\mathbf{G}_\nu$ matrix, which for a given ν is of the dimension $(2\Psi \times 2\Psi)$, is then evaluated from the following equation:

$$\mathbf{G}_\nu = \left(\mathbf{Y_{1}}_{\nu} + \mathbf{Y_{2}}_{\nu}\mathbf{X''_{43}}_{,\nu}\right) {\mathbf{X''}_{\nu}}^{-1} \tag{30}$$

B. Creating the $\mathbf{S}$ *vector*

Similar to the procedure for calculating the $\mathbf{G}$ matrix, the procedure for calculating the $\mathbf{S}$ vector for the structure with an arbitrary number of superstrates and substrates can be derived. To derive the electric fields, tangential to the patches, due to the probe with the patch being absent, we need to impose the continuity conditions on the tangential components of the electric and magnetic fields at the interfaces $\rho = r_2, r_3, \ldots, r_K$. The field expressions in (3) satisfy the boundary condition on the metallic surface at $\rho = r_1$.

The procedure can be outlined as follows:

1) Write the boundary conditions for the tangential components $\tilde{E}_z^\kappa$, $\tilde{E}_\phi^\kappa$, $\tilde{H}_z^\kappa$ and $\tilde{H}_\phi^\kappa$ $(\kappa = 1, \ldots, K-1)$ in the spectral domain at each interface in the form of a set of equations:

$$\begin{aligned} \tilde{E}^\kappa_{(z,\phi)}(\rho = r_{\kappa+1}) &- \tilde{E}^{\kappa+1}_{(z,\phi)}(\rho = r_{\kappa+1}) = 0 \\ \tilde{H}^\kappa_{(z,\phi)}(\rho = r_{\kappa+1}) &- \tilde{H}^{\kappa+1}_{(z,\phi)}(\rho = r_{\kappa+1}) = 0 \end{aligned}$$

2) Rewrite the set of equations in matrix form, which for a chosen number ν takes the following form:

$$\mathbf{P}_\nu \mathbf{B}_\nu = \mathbf{Q}_\nu \tag{31}$$

where $\mathbf{P}_\nu$ is a square matrix of dimension $4(K-1)$, the elements of which are the expressions standing next to unknown coefficients. $\mathbf{B}_\nu$ is a vector of length $4(K-1)$ of the form:

$$\begin{aligned} \mathbf{B}_\nu = \Big[&B^e_{\nu 1}, B^h_{\nu 1}, B^e_{\nu 2}, B^h_{\nu 2}, B'^e_{\nu 2}, B'^h_{\nu 2} \ldots, \\ &B^e_{\nu\kappa}, B^h_{\nu\kappa}, B'^e_{\nu\kappa}, B'^h_{\nu\kappa}, \ldots, B^e_{\nu K}, B^h_{\nu K}\Big]^T \end{aligned}$$

$\mathbf{Q}_\nu$ is a vector of length $4(K-1)$, the elements of which are the integral expressions concerning the probe excitation. Since the field expressions depend on the ρ' value, the elements of matrix $\mathbf{Q}_\nu$ also have a different form and have to be derived for particular cases of the ρ' value. In each region, in the substrate layers, the fields are defined by function 1 (for $r_\kappa \le \rho \le \rho'$) or function 2 (for $\rho' \le \rho \le r_{\kappa+1}$) for $\kappa = 1, 2, \ldots, \kappa_\Psi - 1$. The value of the $\mathbf{Q}_\nu$ matrix elements are calculated by integrating the appropriate expression over the probe length (from r_1 to r_{κ_ψ}). Considering above, the integrated functions have to change when integration path crosses substrate layers. For example, while integrating the expression in the range (r_1, r_2) the continuity condition at interface $\rho = r_2$ has to consider function 2 in both regions. Next, while integrating in the range (r_2, r_3), the continuity condition at interface $\rho = r_2$ has to consider function 1 in both regions.

3) In the next step, we pick the layers for which the unknown coefficients are to be calculated in the function of the coefficients in the other layers. Since the aim of the analysis is to calculate the electric fields in the layers where the patches are located, the most reasonable choice is to pick layers above the patches (layers κ_ψ) or below the patches (layer $\kappa_\psi - 1$). Let us choose the layers located above the patches. In this case, equation (31) needs to be rearranged so that the unknown amplitudes from the chosen layers are moved to the top of the amplitude vector. With these assumptions, the following set of matrix equations is obtained:

$$\mathbf{P'}_{1\nu}\mathbf{B}_{c\nu} + \mathbf{P'}_{2\nu}\mathbf{B}_{r\nu} = \mathbf{Q_{1}}_{\nu} \tag{32}$$

$$\mathbf{P'}_{3\nu}\mathbf{B}_{c\nu} + \mathbf{P'}_{4\nu}\mathbf{B}_{r\nu} = \mathbf{Q_{2}}_{\nu} \tag{33}$$

where vector $\mathbf{B}_{c\nu}$ contains the amplitudes from the κ_ψ layers in the form:

$$\begin{aligned} \mathbf{B}_{c\nu} = \Big[&B^e_{\nu\kappa_1}, B'^e_{\nu\kappa_1}, \ldots, B^e_{\nu\kappa_\Psi}, B'^e_{\nu\kappa_\Psi}, \\ &B^h_{\nu\kappa_1}, B'^h_{\nu\kappa_1}, \ldots, B^h_{\nu\kappa_\Psi}, B'^h_{\nu\kappa_\Psi}\Big]^T \end{aligned}$$

and vector $\mathbf{B}_{r\nu}$ contains all the other amplitudes. Matrices $\mathbf{P'}_{j\nu}$ $(j = 1, \ldots, 4)$ are composed from matrix $\mathbf{P}_\nu$ by rearranging its rows and columns, and are of dimensions: $\mathbf{P'}_{1\nu}$ - $(4\Psi \times 4\Psi)$, $\mathbf{P'}_{2\nu}$ - $(4\Psi \times (4(K-1) - 4\Psi))$, $\mathbf{P'}_{3\nu}$ - $((4(K-1) - 4\Psi) \times 4\Psi)$, and $\mathbf{P'}_{4\nu}$ - $((4(K-1) - 4\Psi) \times (4(K-1) - 4\Psi))$.

4) From (33), the relation between the coefficients $\mathbf{B}_{r\nu}$ and $\mathbf{B}_{c\nu}$ is derived, and substituting it to (32) the amplitude vector in the chosen layer is obtained in the form:

$$\mathbf{B}_{c\nu} = {\mathbf{P''}_{\nu}}^{-1}\mathbf{R}_\nu \tag{34}$$

where:

$$\begin{aligned} \mathbf{P''}_\nu &= \mathbf{P'}_{1\nu} - \mathbf{P'}_{2\nu}{\mathbf{P'}_{4\nu}}^{-1}\mathbf{P'}_{3\nu} \\ \mathbf{R}_\nu &= \mathbf{Q_{1}}_{\nu} - \mathbf{P'}_{2\nu}{\mathbf{P'}_{4\nu}}^{-1}\mathbf{Q_{2}}_{\nu} \end{aligned}$$

5) In order to calculate the spectral-domain transverse components of the electric fields in regions κ_ψ, the following matrix equation is derived:

$$\begin{aligned} \begin{bmatrix} \tilde{\mathbf{E}}^{feed}_{\phi\nu}(k_z) \\ \tilde{\mathbf{E}}^{feed}_{z\nu}(k_z) \end{bmatrix} &= \mathbf{M}_\nu \mathbf{B}_{c\nu} + \mathbf{O}_\nu = \\ = \mathbf{M}_\nu {\mathbf{P''}_{\nu}}^{-1}\mathbf{R}_\nu + \mathbf{O}_\nu &= \mathbf{T}_\nu \mathbf{R}_\nu + \mathbf{O}_\nu = \mathbf{S}_\nu \end{aligned} \tag{35}$$

where $\mathbf{M}_\nu$ is a $2\Psi \times 4\Psi$ matrix of which the elements are the expressions standing next to the unknown coefficients in the κ_ψ regions, and $\mathbf{O}_\nu$ is a vector of length 2Ψ containing integral expressions concerning the probe excitation. Note that in region Ψ there are no probes and therefore the elements of vector $\mathbf{O}_\nu$ corresponding to this region are equal to zero.

APPENDIX B
MATRICES FOR ANTENNA IMPEDANCE AND RADIATION PATTERN

Vector $\mathbf{G}'^{\kappa}_{\nu}(\cdot)$ from (20) has the following form:

$$\mathbf{G}'^{\kappa}_{\nu} = \left(\begin{bmatrix} D^{\rho,\kappa}_{1,\nu} & D^{\rho,\kappa}_{2,\nu} \end{bmatrix} + \begin{bmatrix} D^{\rho,\kappa}_{3,\nu} & D^{\rho,\kappa}_{4,\nu} \end{bmatrix} \mathbf{W}^{''\kappa}_{43\nu}\right) {\mathbf{W}''^{\kappa}_{\nu}}^{-1} \tag{36}$$

where

$$D_{1,\nu}^{\rho,\kappa} = \begin{cases} \frac{k_z}{k_{1\rho}} \left(H_{\nu 1}^{'\rho} - \frac{H_{\nu 1}^{r_1}}{J_{\nu 1}^{r_1}} J_{\nu 1}^{'\rho} \right), & \kappa = 1 \\ \frac{k_z}{k_{\kappa\rho}} H_{\nu\kappa}^{'\rho}, & \kappa = 2, \ldots, \kappa' - 1 \end{cases}$$

$$D_{2,\nu}^{\rho,\kappa} = \begin{cases} \frac{i\omega\mu_0\nu}{k_{1\rho}^2\rho} \left(H_{\nu 1}^{\rho} - \frac{H_{\nu 1}^{'r_1}}{J_{\nu 1}^{'r_1}} J_{\nu 1}^{\rho} \right), & \kappa = 1 \\ \frac{i\omega\mu_0\nu}{k_{\kappa\rho}^2\rho} H_{\nu\kappa}^{\rho}, & \kappa = 2, \ldots, \kappa' - 1 \end{cases}$$

$$D_{3,\nu}^{\rho,\kappa} = \frac{k_z}{k_{\kappa\rho}} J_{\nu\kappa}^{'\rho}, \quad \kappa = 2, \ldots, \kappa' - 1$$

$$D_{4,\nu}^{\rho,\kappa} = \frac{i\omega\mu_0\nu}{k_{\kappa\rho}^2\rho} J_{\nu\kappa}^{\rho}, \quad \kappa = 2, \ldots, \kappa' - 1 \tag{37}$$

and matrices $\mathbf{W}_{\nu}^{''\kappa}$ and $\mathbf{W}_{43\nu}^{''\kappa}$ are of dimensions 2×2, and are calculated in similar way as matrices $\mathbf{X}_{\nu}^{''}$ in (27) and $\mathbf{X}_{43\nu}^{''}$ in (28) by selecting the chosen amplitudes $\mathbf{A}_{c\nu} = [A_{\nu\kappa}^{e}, A_{\nu\kappa}^{h}]^T$ for $\kappa = 1, \ldots, \kappa' - 1$. Note that for the first layer ($\kappa = 1$) matrix $\mathbf{W}_{43\nu}^{''1}$ and elements $D_{3,\nu}^{\rho,1}$ and $D_{4,\nu}^{\rho,1}$ do not exist.

The elements of matrix $\mathbf{\Gamma}_{\nu}$ from (21) depend on the location of the patch antennas in the structure. In the case of patch antennas located only on the top layer at $\rho = r_K$:

$$\mathbf{\Gamma}_{\nu}(\cdot) = \mathbf{X''}_{\nu}^{-1}(\cdot)$$

where $\mathbf{X''}_{\nu}$ is defined in (27), and in this case is of dimension 2×2. If the patch antennas are located on the top layer at $\rho = r_K$ and other $\Psi - 1$ layers at $\rho = r_{\kappa_\psi}$ ($\kappa_\psi < K$), matrix $\mathbf{\Gamma}_{\nu}$ is of dimension $2 \times 2\Psi$ and is composed from matrix $\mathbf{X''}_{\nu}^{-1}$ by selecting those rows related to the coefficients $A_{\nu,K}^{e}$ and $A_{\nu,K}^{h}$. In the case when the patches are covered by superstrate layers (there are no patch antennas on the top layer), matrix $\mathbf{\Gamma}_{\nu}$ is defined as follows:

$$\mathbf{\Gamma}_{\nu}(\cdot) = \mathbf{X'''}_{43,\nu}(\cdot)\mathbf{X''}_{\nu}^{-1}(\cdot)$$

where $\mathbf{X'''}_{43,\nu}$ is a $2 \times 2\Psi$ matrix composed from matrix $\mathbf{X''}_{43,\nu}$ by selecting those rows related to the coefficients $A_{\nu,K}^{e}$ and $A_{\nu,K}^{h}$.

REFERENCES

[1] L. Josefsson and P. Persson, *Conformal Array Antenna Theory and Design*. Hoboken: John Wiley and Sons, Inc., 2006.

[2] J. R. Wait, *Electromagnetic Radiation from Cylindrical Structures*. London: Pergamon Press, 1959.

[3] G. Stewart and K. Golden "Mutual admittance for axial rectangular slots in a large conducting cylinder," *IEEE Trans. Antennas Propag.*, vol. 19, no. 1, pp. 120–122, Jan. 1971.

[4] R. F. Harrington, *Time Harmonic Electromagnetic Fields*. Prentice-Hall, 1961.

[5] P. Persson and R.G. Rojas, "Efficient technique for mutual coupling calculations between apertures on a PEC circular cylinder covered with a dielectric layer," *IEEE Antennas and Propag. Soc. Intern. Symp.*, vol. 3, pp. 252–255, Jul. 2001.

[6] Z. Sipus *et al.*, "An algorithm for calculating Green's functions of planar, circular cylindrical and spherical multilayer substrates," *App. Computational Electromag. Soc. Journal*, vol. 13, no. 3, pp. 243-254, 1998.

[7] A. F. Peterson and R. Mittra "Mutual admittance between slots in cylinders of arbitrary shape," *IEEE Trans. Antennas Propag.*, vol. 37, no. 7, pp. 858–864, Jul 1989.

[8] Z. Sipus *et al.*, "Moment method analysis of circular-cylindrical array of waveguide elements covered with a radome," *IEEE Antennas and Propag. Soc. Intern. Symp.*, vol. 2, pp. 350–353, Jul. 2001.

[9] C. M. da Silva and J. C. daS. Lacava, "Mutual impedance of conformal cylindrical microstrip antenna arrays with a protection layer," *1995 SBMO/IEEE MTT-S Intern. Microw. and Optoelectr. Conference, 1995. Proc.*, vol. 1, pp. 314–319, Jul. 1995.

[10] R. C. Acar, and G. Dural, "Mutual coupling of printed elements on a cylindrically layered structure using closed-form green's functions," *Prog. Electromagn. Res.*, vol. 78, pp. 103–127, 2008.

[11] Q.-Q. He, and B.-Z. Wang, "Radiation patterns synthesis for a conformal dipole antenna array," *Prog. Electromagn. Res.*, Vol. 76, pp. 327–340, 2007.

[12] M. He and X. Xu, "Closed-form solutions for analysis of cylindrically conformal microstrip antennas with arbitrary radii," *IEEE Trans. Antennas Propag.*, vol. 53, no. 1, pp. 518–525, Jan. 2005.

[13] D. Khedrouchea *et al.* "Spectral-domain analysis of multilayer cylindricalrectangular microstrip antennas," *Engineering Analysis with Boundary Elements*, vol. 33, no. 7, pp. 930-939, Jul. 2009.

[14] S. M. Ali *et al.*, "Resonance in cylindrical-rectangular and wraparound microstrip structures," *IEEE Trans. Microw. Theory Techn.*, vol. 37, no. 11, pp. 1773–1783, Nov. 1989.

[15] T. M. Habashy *et al.*, "Input impedance and radiationpattern of cylindrical-rectangular and wraparound microstrip antennas," *IEEE Trans. Antennas Propag.*, vol. 38, no. 5, pp. 722–731, May 1990.

[16] K.-L. Wong *et al.*, "Resonance in a superstrate-loaded cylindrical-rectangular microstrip structure," *IEEE Trans. Microw. Theory Techn.*, vol. 41, no. 5, pp. 814–819, May 1993.

[17] Kin-Lu Wong *et al.*, "Analysis of a cylindrical-rectangular microstrip structure with an airgap," *IEEE Trans. Microw. Theory Techn.*, vol. 42, no. 6, pp. 1032–1037, Jun. 1994.

[18] S. Karan and V. B. Erturk, "Closed-form green's functions in cylindrically stratified media for method of moments applications," *2009. ICEAA '09. Intern. Conference on Electromag. in Advanced Applications*, pp. 473–476, 14-18 Sep. 2009.

[19] S.-Y. Ke and K.-L. Wong, "Input impedance of a probe-fed superstrate-loaded cylindrical-rectangular microstrip antenna," *Microw. Opt. Technol. Lett.*, vol. 7, pp. 232-236, 1994.

[20] S. Raffaelli *et al.*, "Analysis and measurements of conformal patch array antennas on multilayer circular cylinder," *IEEE Trans. Antennas Propag.*, vol. 53, no. 3, pp. 1105–1113, Mar. 2005.

[21] L. C. Kempel *et al.*, "Radiation by patch antennas on a circular cylinder using the FE-BI method," *Antennas and Propag. Soc. Intern. Symp., 1994. AP-S. Digest,*, vol. 1, pp. 182–185, Jun. 1994.

[22] T. Rylander and A. Bondeson, "Application of stable FEM-FDTD hybrid to scattering problems," *IEEE Trans. Antennas Propag.*, vol. 50, no. 2, pp. 141–144, Feb. 2002.

[23] W. Yu and R. Mittra, "A conformal FDTD software package modeling antennas and microstrip circuit components," *IEEE Antennas Propag. Mag.*, vol. 42, no. 5, pp. 28–39, Oct. 2000.

[24] He Mang and Xu Xiaowen, "Full-wave analysis and wide-band design of probe-fed multilayered cylindrical-rectangular microstrip antennas," *IEEE Trans. Antennas Propag.*, vol. 52, no. 7, pp. 1749–1757, Jul. 2004.

[25] I. J. Craddock *et al.*, "Cylindrical-Cartesian FDTD model of a 17-element conformal antenna array," *Electr. Lett.*, vol. 37, no. 24, pp. 1429–1431, Nov. 2001.

[26] R. Abou-Jaoude and E. K. Walton, "Numerical modeling of on-glass conformal automobile antennas," *IEEE Trans. Antennas Propag.*, vol. 46, no. 6, pp. 845–852, Jun. 1998.

[27] V. B. Erturk *et al.*, "Analysis of finite arrays of axially directed printed dipoles on electrically large circular cylinders," *IEEE Trans. Antennas Propag.*, vol. 52, no. 10, pp. 2586–2595, Oct. 2004.

[28] B. Thors and L. Josefsson, "Radiation and scattering tradeoff design for conformal arrays," *IEEE Trans. Antennas Propag.*, vol. 51, no. 5, pp. 1069–1076, May 2003.

[29] P. Persson and L. Josefsson, "Calculating the mutual coupling between apertures on a convex circular cylinder using a hybrid UTD-MoM method," *IEEE Trans. Antennas Propag.*, vol. 49, no. 4, pp. 672–677, Apr. 2001.

[30] W. C. Chew, *Waves and Fields in Inhomogeneous Media*, New York: Van Nostrand, 1990.

[31] C. Tokgoz and G. Dural, "Closed-form Green's functions for cylindrically stratified media," *IEEE Trans. Microw. Theory Techn.*, vol. 48, no. 1, pp. 40–49, Jan. 2000.

[32] J. S. Dahele *et al.*, "Effect of curvature on characteristics of rectangular patch antenna," *Electr. Lett.* , vol. 23, no. 14, pp. 748–749, Jul. 1987.

[33] G. Franceschetti *et al.*, "Array synthesis with excitation constraints," *Antennas and Propag. Soc. Intern. Symp*, 1988. AP-S. Digest, vol. 3, pp. 1192–1195, 6-10 Jun. 1988.

Rafal Lech was born in Elblag, Poland, in 1977. He received the M.Sc.E.E. and Ph.D. (with honors) degrees from the Gdansk University of Technology, Gdansk, Poland, in 2001 and 2007, respectively. His main research interests are electromagnetic-wave scattering, numerical methods, filter design, complex materials, metamaterial applications at microwave frequencies, electromagnetic analysis of periodic structures, and antenna design.

Wojciech Marynowski was born in Bydgoszcz, Poland, in 1980. He received the M.Sc.E.E. and Ph.D. (with honors) degrees from the Gdansk University of Technology, Gdansk, Poland, in 2004 and 2011, respectively. His research interests include electromagnetic wave propagation in complex materials, design of nonreciprocal planar microwave devices, wideband/ultra-wideband antennas and theirs feeding systems.

Adam Kusiek was born in Mragowo, Poland, in 1980. He received the M.Sc.E.E. and Ph.D. (with honors) degrees from the Gdansk University of Technology, Gdansk, Poland, in 2004 and 2011, respectively. His research interests include developing of hybrid techniques to the analysis of complex structures, electromagnetic wave scattering, integrated nonreciprocal devices, antennas and passive structures for antenna feeding systems.

Jerzy Mazur was born in Brno, Czech Republic, in 1946. He received the M.Sc.E.E., Ph.D., and D.Sc. degrees from the Gdansk University of Technology, Gdansk, Poland, in 1968, 1976, and 1983, respectively. He is currently a Full Professor with Gdansk University of Technology. Since 1992, he has also been a consultant with the Telecommunication Research Institute, Gdansk, Poland. His research interests concern electromagnetic field theory and integrated circuits for microwave and millimeter-wave applications.